Appl. Phys. B 81, 393–402 (2005)
DOI: 10.1007/s00340-005-1892-4

Applied Physics B
Lasers and Optics

M. SCALORA[1,✉]
G. D'AGUANNO[2]
N. MATTIUCCI[2,3]
M.J. BLOEMER[1]
J.W. HAUS[4]
A.M. ZHELTIKOV[5]

Negative refraction of ultra-short electromagnetic pulses

[1]Charles M. Bowden Research Center, AMSRD-AMR-WS-ST, RDECOM, Redstone Arsenal, AL 35898-5000, USA
[2]Time Domain Corporation, Cummings Research Park, 7057 Old Madison Pike, Huntsville, AL 35806, USA
[3]Università 'Roma Tre', Dipartimento di Fisica 'E. Amaldi', Via Della Vasca Navale 84, 00146 Rome, Italy
[4]Electro-Optics Program, University of Dayton, Dayton, OH 45469-0245, USA
[5]Physics Department and International Laser Center, M.V. Lomonosov Moscow State University, Vorob'evy Gory, 119899 Moscow, Russian Federation

Received: 17 March 2005 / Revised version: 14 May 2005
Published online: 15 July 2005 • Springer-Verlag 2005

ABSTRACT We study pulse propagation across a boundary that separates an ordinary medium from a medium with simultaneously negative dielectric permittivity and magnetic permeability. Solving Maxwell's equations with two spatial coordinates (one longitudinal, one transverse) and time we find negative refraction as the wave packet undergoes significant and unusual shape distortions. The pulse acquires and maintains a chirp as it traverses the interface, as expected, but with a sign that is opposite to the chirp attained upon traversal into a positive-index material. Both a direct calculation of the spatial derivative of the instantaneous, local phase of the pulse and a Fourier analysis of the signal reveal the same inescapable fact: that inside a negative-index material, a *transmitted, forward-moving* wave packet is indeed a superposition of *purely negative* wave vectors. The central findings of this paper are a confirmation that causality is not violated in the short-pulse regime, and that energy and group velocities never exceed the speed of light in vacuum.

PACS 42.25.Bs; 42.25.Gy; 78.20.Ci

1 Introduction

Following the breakthrough idea of negative-index materials, or NIMs, a new chapter is currently being written in the field of optics. As Veselago first postulated [1], if the dielectric susceptibility ε and the magnetic permeability μ are simultaneously negative, one must then allow for the possibility that the index of refraction, defined as $n = \pm\sqrt{\varepsilon\mu}$, may in fact be negative. As a result, light can act in a seemingly peculiar way: Snell's law remains valid for negative n, and refraction is predicted to occur at negative angles, well beyond the normal, in the quadrant opposite to the direction of refraction associated with common materials. Related effects of this distinctive dynamics include a Poynting vector $\boldsymbol{S}$ and the wave vector $\boldsymbol{k}$ directed in opposite directions [1], at least for incident plane waves ($\boldsymbol{S}$ points in the direction away from the source, while $\boldsymbol{k}$ points toward it), and a seemingly negative energy density [1]. While it is not unusual for the Poynting vector not to be collinear with the wave vector (e.g. in regions close to a source of finite size, where the wavefront is not plane), early on Veselago realized that such a medium could exist if it displayed material dispersion. He reasoned that this requirement would be enough to avoid the energy inconsistency and other inherent anomalies associated with a negative energy.

Veselago's predictions remained only within the realm of possibilities until recent experimental observations [2] appeared to confirm the effect. The experiments were carried out with microwaves on a composite system of so-called split-ring resonators [3], which in combination with other metallic components yield simultaneously negative, effective ε and μ. A brief review of the current literature reveals that since Pendry's predictions [4] that these materials may act as unusual super-lenses, free of the shortcomings associated with ordinary glass lenses, that may even restore evanescent waves, the subject matter has been strenuously debated [5–7]. Although much of the controversy has now subsided, objections centered around a few basic points: (i) do Maxwell's equations actually support this type of solution? (ii) Is momentum conserved? (iii) Is causality violated, as it appears that parts of the beam would have to travel faster than the speed of light to catch up with the rest of the beam? (iv) Will absorption ultimately prove to be too much for the effect to ever be observable? (v) What is the sign of the group velocity? Nevertheless, the debate has not stopped many workers from reporting different aspects of the dynamics involving NIMs that range from causality [8] and superluminal propagation [9], to two-dimensional propagation that includes material dispersion [10]. Other subjects tackled include wavefront distortions of steady-state transverse Gaussian beams [11], modification of quantum-mechanical spontaneous and stimulated emission rates [12], multilayer NIM stacks [13], nonlinear interactions [14], and propagation in guiding layers surrounded by a NIM [15]. A number of additional works that span the field can be found in a focus issue of Optics Express published in 2003 [16].

✉ Fax: +1-256-955-7216, E-mail: michael.scalora@us.army.mil

It has also been shown that light can be negatively refracted (perhaps *scattered* may be a more apt term) as it passes through a photonic band gap (PBG) structure that has a negative effective index of refraction [17, 18]. Because negative-index materials are not known to occur naturally, the manifestation of this phenomenon in positive-index materials makes it possible to begin detailed studies of the effects that appear to characterize NIMs. Although the effective index of refraction of structures that have complicated topologies may indeed be negative, in drawing these analogies one always runs the risk of carrying them too far, and so some care should always be exercised, in view of the fact that so far no rigorous justification has been provided.

The controversial debate that has characterized this field is the motivating factor behind this work. Our approach is pedagogical in nature, as we consider the spatio-temporal dynamics of short pulses that are localized in space and time, under conditions of both normal and oblique incidence. The dynamics of pulses can be very different, far richer, and more telling than the interference of continuous-wave beams [11]. In fact, under pulsed conditions, we predict that upon traversal of a NIM interface a pulse re-shapes considerably and acquires a chirp opposite in sign to the chirp imparted when the pulse crosses an ordinary interface. In other words, in this regime the initial wave packet, which is localized in space, broadens significantly in Fourier space under the action of geometrical dispersion (dispersion due to the scattering process), as a range of *purely negative wave vectors* are created inside the NIM, in a process strongly reminiscent of a scattering event, even though actual reflections may be small. The bandwidth of the transmitted wave packet broadens in k-space with increasingly more negative ε and μ, but remains unaltered as it propagates further into the NIM. Material dispersion, which is assumed to be present, only affects the group velocity, and plays no other role primarily because the propagation distances that we consider are short.

The generation of negative wavenumbers is usually associated with reflected or backward-propagating components. A Fourier analysis of the incident and scattered pulses immediately reveals all constituent, instantaneous wave vectors in the form of wave packets of finite width, centered at the respective input and scattered carrier wave vectors, each with the appropriate sign: positive for forward propagation, negative for reflection. Although these effects may be commonplace and may be second nature to most, these simple linear effects are almost never discussed in the literature, and so we show a simple example of one such occurrence in Fig. 1, where we show the spectrum of the input and scattered fields as a 100-fs pulse traverses the interface that separates vacuum from a dispersion-less material of index $n = 3$. The k-space bandwidth of the transmitted wave packet increases by approximately a factor of n, to reflect the spatial compression that the pulse undergoes in physical space as it enters the high-index medium. The inclusion of linear dispersion generally changes the group velocity of the transmitted pulse, which in turn alters the degree of broadening of the transmitted wave packet in k-space. Therefore, this effect arises because a pulse crosses a physical boundary (geometrical dispersion), is not due to material dispersion, and the pulse is left with a small chirp. In contrast, the unusual byproduct of the dynamics of a pulse transiting into a NIM is completely out of the ordinary, with electromagnetic energy and momentum that keep moving forward, while the spatial frequencies that make up the pulse are all negative. Given the oddity of this situation, it is not surprising to find results that may appear strange and counterintuitive at first, or flatly wrong as claimed by some.

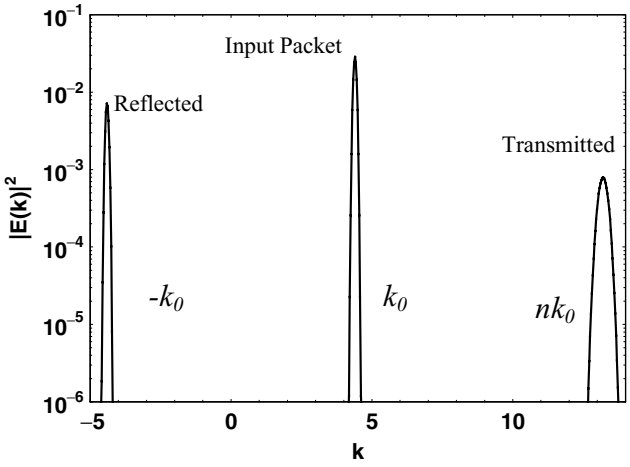

FIGURE 1 Input, reflected, and transmitted wave packets for a 100-fs pulse incident on a dispersion-less medium of index $n = 3$. The transmitted wave packet broadens by a factor of n as a result of spatial compression that the fields undergo. As expected, the reflected pulse has the same bandwidth as the incident pulse. For materials that display normal, linear material dispersion, the transmitted wave packet will display additional broadening due to additional slow-down, which further compresses the pulse in space

The study of layered, one-dimensional PBG structures has taught us that geometrical dispersion, which arises from the introduction of spatial inhomogeneities in the index of refraction (interfaces), can be controlled and made to compensate for material dispersion in a way that makes it possible, for example, to obtain exactly phase-matched nonlinear frequency conversion from naturally dispersive, unmatchable materials [19]. In the same vein, it has been amply demonstrated that absorption does not necessarily follow from having a large imaginary index of refraction. In fact, even hundreds of nanometers of silver metal can become transparent (transmission well above 50%) in the visible range and beyond, provided that metal layers are appropriately spaced [20]. Therefore, one cannot exclude a priori the possibility that a clever scheme will not be devised, that perhaps includes layered, absorbing NIMs, arranged to yield geometrical dispersion to compensate material dispersion [19], or perhaps suppress metal-like absorption [20], to make Pendry's super-lens and other effects possible, despite predictions to the contrary [5].

Our approach reveals new dynamical aspects that we hope will help shed new light on the matter, and help to overcome, at least partially, even the strongest objection registered to date, namely, that causality is manifestly violated [6]. In Refs. [6] and [21], for example, the authors (VM&V) vigorously assert that in order for negative refraction to occur causality would necessarily have to be violated because part of the beam would have to travel at superluminal group velocities, both in vacuum and inside the medium.

This argument is used by the authors in Ref. [6] to reject any notion that the effect may manifest itself under any conditions.

Using a novel pulse-propagation method, the central finding of this paper is a confirmation of the effect in the short-pulse regime. We will show that an input pulse refracts in the negative direction after impinging upon a NIM, as predicted by Veselago and as argued by Pendry. As the pulse is compressed sideways with respect to the direction of propagation, traversal into the NIM is accompanied by significant pulse distortions and a re-orientation of the phase planes that conspire to pre-empt superluminal energy or group velocities. Given this out-of-the-ordinary dynamics, we take a necessary step back and seek to establish simple facts about NIMs in order to gain some rudimentary understanding of the electrodynamics associated with the transit of well-localized wave packets from a region of positive-index material into a NIM.

2 The Drude model and the field equations

We begin our analysis by writing the dispersion relations for a Drude medium, as set forth in Ref. [1], for example. The absence of resonances makes it possible to operate in regions of the spectrum where absorption is negligible, provided propagation distances are limited:

$$\mu(\omega) = \varepsilon(\omega) = 1 - \frac{\omega_{\rm p}^2}{\omega^2}. \tag{1}$$

For simplicity, we have chosen the same plasma frequencies for both ε and μ. Beginning from a dispersion relation, one usually needs to produce the time derivatives $\partial \mathbf{D}(\mathbf{r}, t)/\partial t$ and $\partial \mathbf{B}(\mathbf{r}, t)/\partial t$ in order to write Maxwell's equations. The alternative approach is to directly couple the material equations of motion for the polarization and magnetization to Maxwell's equations in the time domain [8–10]. However, it is instructive to proceed in this fashion because the approach provides useful insight into the dynamics unavailable with other methodologies. Assuming that $\mathbf{D}$ is linearly polarized, we write it in complex notation in the usual manner: $\mathbf{D} = \mathbf{i}(\, D_{\rm x}(\mathbf{r}, t) \,+ \text{c.c.})$. We now assume that the dispersion function is approximately linear in the region of interest, and that it can be written in the form $\varepsilon(\omega) \approx \varepsilon(\omega_0) + \alpha(\omega - \omega_0)$ in the neighborhood of ω_0. Then, the constitutive relation that relates the displacement vector to the electric field takes the form

$$D_{\rm x}(\mathbf{r}, t) = (\varepsilon(\omega_0) - \alpha\omega_0)\, E_{\rm x}(\mathbf{r}, t) {\rm e}^{-{\rm i}\omega t} + {\rm i}\alpha \frac{\partial}{\partial t} \left(E_{\rm x}(\mathbf{r}, t) {\rm e}^{-{\rm i}\omega t} \right). \tag{2}$$

The calculation of $\partial D_{\rm x}(\mathbf{r}, t)/\partial t$ is straightforward. The result is [22, 12]

$$\frac{\partial D_{\rm x}}{\partial t} = -{\rm i}\omega\varepsilon(\omega) E_{\rm x} + \frac{\partial\, [\, \omega\varepsilon(\omega)\,]}{\partial \omega} \frac{\partial E_{\rm x}}{\partial t}, \tag{3}$$

where $\partial\, \varepsilon(\omega)\, /\partial\omega = \alpha$, and we have neglected higher-order time derivatives. The neglect of higher-order terms in the power-series expansion for the permittivity (and permeability) implies that Eq. (3) is valid if the dispersion function is relatively smooth in the region of interest. This is in fact a good approximation for the Drude model, which lacks resonances, as well as the Lorentz model if the carrier frequency is tuned some distance away from any resonance peak, where one would also have to contend with absorption. Alternatively, a first-order power-series expansion is always valid if the bandwidth of the incident pulse is narrow enough, or if propagation distances are short in order to prevent pulse re-shaping. In the absence of any resonances, this usually means a few tens of wave cycles. If on the other hand higher-order terms must be included, higher-order temporal derivatives of the electric field envelope would necessarily have to find their way into Eq. (3).

Relationships similar to Eq. (3) can also be derived for the components of the fields $\mathbf{B}$ and $\mathbf{H}$. Therefore, in the presence of approximately linear dispersion, the generalized energy density takes the form [22]

$$U = \frac{1}{8\pi} \left(\frac{\partial\, [\, \omega\varepsilon(\omega)\,]}{\partial\omega} |\mathbf{E}|^2 + \frac{\partial\, [\, \omega\mu(\omega)\,]}{\partial\omega} |\mathbf{H}|^2 \right), \tag{4}$$

where both ε and μ may be functions of position. At first sight the assumptions that lead to this form of energy density appear to be restrictive when it comes to pulse duration, if ε and μ have any meaningful curvature. At the same time, Eq. (4) seems to give physically reasonable and meaningful results even for pulses that are only a few wave cycles in duration, as long as the dispersion curves do not vary too rapidly with frequency. So, in what follows we will use pulses a few tens of optical cycles in duration, but will not assume slowly varying field amplitudes. Mindful of its limitations, we will continue to use the energy density defined in Eq. (4) to get a handle on the restrictions that causality imposes on the energy velocity, but calculations are carried out regardless of whether or not Eq. (4) is valid. In any case, one should always be mindful of the fact that unless ε and μ are constants in time and dispersionless, it is not generally possible to write an expression for the energy density in closed form [22, 23].

According to Eq. (4), the requirement that energy be positive calls for [1] $\partial\, [\, \omega\varepsilon(\omega)\,]/\partial\omega > 0$ and $\partial\, [\, \omega\mu(\omega)\,]/\partial\omega > 0$ to be simultaneously satisfied. Equations (1) satisfy these conditions. So the Drude model yields simultaneously negative ε and μ for frequencies just below the plasma frequency, while at the same time ensuring that the energy density in Eq. (4) remains positive.

In Fig. 2 we show the geometrical arrangement of our system. A pulse is initially located in vacuum, some distance away from an interface that separates two generic materials. The electric field is linearly polarized, points into the page, and is incident at an arbitrary angle $\theta_{\rm i}$. We expand the fields as follows:

$$\begin{aligned} \mathbf{E} &= \mathbf{i}\big(E_{\rm x}(y, z, t)\, {\rm e}^{{\rm i}(k_{\rm z} z - k_{\rm y} y - \omega t)} + \text{c.c.}\big), \\ \mathbf{H} &= \mathbf{j}\big(H_{\rm y}(y, z, t)\, {\rm e}^{{\rm i}(k_{\rm z} z - k_{\rm y} y - \omega t)} + \text{c.c.}\big) \\ &\quad + \mathbf{k}\big(H_{\rm z}(y, z, t)\, {\rm e}^{{\rm i}(k_{\rm z} z - k_{\rm y} y - \omega t)} + \text{c.c.}\big), \end{aligned} \tag{5}$$

where $k_{\rm z} = |\mathbf{k}| \cos\theta_{\rm i}$ and $k_{\rm y} = -|\mathbf{k}| \sin\theta_{\rm i}$, $|\mathbf{k}| = k_0 = \omega/c$. This choice of carrier wave vector is consistent with the fact that the pulse is initially located in vacuum. We make no other assumptions about the envelope functions, which

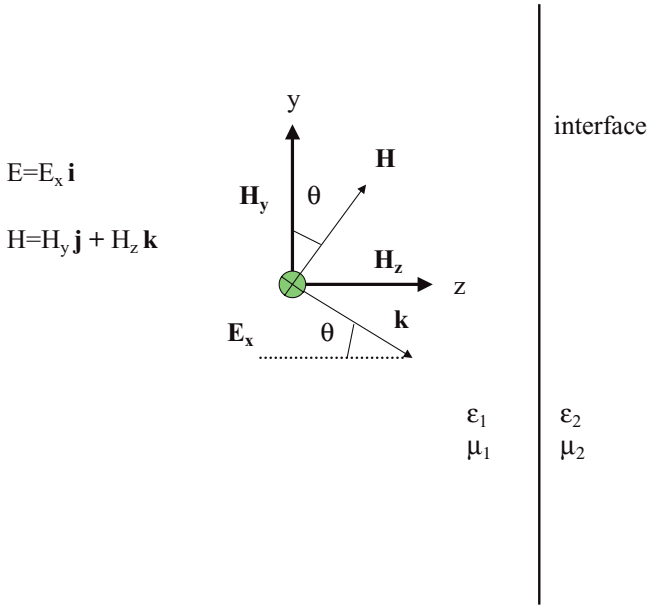

FIGURE 2 Geometric arrangement of our system. The pulse is initially located on the left-hand side of an interface which separates two generic media. The electric field is polarized into the page. At oblique incidence this setup yields two magnetic field components, one transverse and one longitudinal with respect to the direction of propagation. The pulse-propagation algorithm that we use can easily be adjusted to include incident TM-polarized pulses

are substituted into the vector Maxwell's equations and are allowed to evolve according to whatever physical boundaries and media are present within the spatial grid. Thus, the field's phase is allowed to evolve free of preconditions, as a function of position and time. Using Eq. (5), we can explicitly write out the Poynting vector in terms of the field envelope functions. It will have two components in the y–z plane:

$$\mathbf{S} = \frac{c}{4\pi}\mathbf{E}\,x\,\mathbf{H} = \mathbf{k}\,S_z(y,z,t) + \mathbf{j}S_y(y,z,t)$$
$$= \frac{c}{4\pi}\left(\mathbf{k}\left(E_x H_y^* + E_x^* H_y\right) - \mathbf{j}\left(E_x H_z^* + E_x^* H_z\right)\right). \quad (6)$$

Then, using Eqs. (4) and (6) we can easily calculate the energy velocity as [23]

$$\mathbf{V}_E = \frac{<\mathbf{S}>}{<U>} = c\,\frac{\left\langle \mathbf{k}\left(E_x H_y^* + E_x^* H_y\right) - \mathbf{j}\left(E_x H_z^* + E_x^* H_z\right)\right\rangle}{\left\langle \frac{\partial[\omega\varepsilon(\omega)]}{\partial\omega}|E_x|^2 + \frac{\partial[\omega\mu(\omega)]}{\partial\omega}(|H_y|^2 + |H_z|^2)\right\rangle}. \quad (7)$$

The brackets indicate that spatial averages should be performed over the volume of interest.

At this point we purposely avoid making the identification between energy and group velocity. Although the two velocities are the same for homogenous media, away from any boundaries, and even inside uniformly layered, one-dimensional structures of infinite length [24], the two are generally *not* the same near surfaces or inside strongly scattering elements, such as PBG structures of finite size [25]. In fact, it has been shown that the group velocity can be negative or superluminal while the energy velocity always remains well below the speed of light in vacuum. The discrepancy between the two velocities is usually associated with pulse re-shaping and scattering losses due to the geometrical dispersion that arises as one introduces index discontinuities [25]. Nevertheless, the physical difference between group and energy velocity is generally not recognized, and in all the literature cited the terms are used interchangeably. Even if group velocities were to become negative or superluminal, as it may easily occur under extreme or unusual conditions, it should not become a point of contention or concern because its physical meaning would then be in need of reassessment. So, abundant caution should always be exercised before one is tempted to interpret such a velocity as the velocity at which energy flows, especially if finite structures are involved, and, just as phase velocity is put in its place when the need arises, so should the group velocity. One should be mindful of these considerations, in view of the sort of objections that have been raised in this regard [5, 6], and especially if multiple NIM interfaces are treated. With this final note of caution, we substitute Eqs. (3) and (5) into the vector Maxwell's equations:

$$\nabla\times\mathbf{E} = -\frac{1}{c}\frac{\partial\mathbf{B}}{\partial t},$$
$$\nabla\times\mathbf{H} = \frac{1}{c}\frac{\partial\mathbf{D}}{\partial t}, \quad (8)$$

and obtain a set of three coupled equations for the field envelopes:

$$\frac{\partial[\tilde{\omega}\varepsilon(\xi)]}{\partial\tilde{\omega}}\frac{\partial E_x}{\partial\tau} = 2\pi\tilde{\omega}\mathrm{i}\left(\varepsilon(\xi)E_x - H_z\sin\theta_i - H_y\cos\theta_i\right) + \frac{\partial H_z}{\partial\tilde{y}} - \frac{\partial H_y}{\partial\xi},$$
$$\frac{\partial[\tilde{\omega}\mu(\xi)]}{\partial\tilde{\omega}}\frac{\partial H_y}{\partial\tau} = 2\pi\tilde{\omega}\mathrm{i}\left(\mu(\xi)H_y - E_x\cos\theta_i\right) - \frac{\partial E_x}{\partial\xi},$$
$$\frac{\partial[\tilde{\omega}\mu(\xi)]}{\partial\tilde{\omega}}\frac{\partial H_z}{\partial\tau} = 2\pi\tilde{\omega}i\left(\mu(\xi)H_z - E_x\sin\theta_i\right) + \frac{\partial E_x}{\partial\tilde{y}}. \quad (9)$$

To summarize, Eqs. (9) are new, and were derived beginning from the vector Maxwell's equations using two rather simple but not too restrictive assumptions: (i) that dispersion is substantially linear in the region of interest and (ii) that absorption is negligible. We have used the scaled coordinates: $\xi = z/\lambda_p$; $\tilde{x} = x/\lambda_p$; $\tau = ct/\lambda_p$. We have also scaled the frequency as $\tilde{\omega} = \omega/\omega_p$, where λ_p is conveniently chosen to be the wavelength associated with the plasma frequency. Both ε and μ are allowed to be spatially dependent. Equations (9) are then solved in the time domain using a modified fast Fourier transform pulse propagation method designed to handle spatial discontinuities [26]. We will not dwell on the merits of the particular method of integration here, except to say that it is unconditionally stable [27], converges rapidly, and is relatively easy to implement as it involves multiplication of linear operators [26].

Now a note on the form of Eqs. (9). For the special case $\varepsilon = \mu$ and for a *homogenous* medium without spatial discontinuities (i.e. away from interfaces), a simple inspection of the equations and the coefficients of the time derivatives immediately reveals the group velocity, $V_G = c/(\partial[\omega\varepsilon(\omega)]/\partial\omega)$. Thus, with the benefit of Eqs. (9)

and the condition that energy should also always be positive, we conclude that the group velocity must always be positive for any material, including NIMs, as long as the material is somewhat transparent. Therefore, using simple energetic arguments the sign of the group velocity is never ambiguous. In the more general case $\varepsilon \neq \mu$, one may also proceed without the benefit of Eqs. (9) as follows: beginning with the inequalities $\partial\,[\,\omega\varepsilon(\omega)\,]/\partial\omega > 0$ and $\partial\,[\,\omega\mu(\omega)\,]/\partial\omega > 0$, we expand them as $\omega(\partial\,\varepsilon/\partial\omega) + \varepsilon > 0$ and $\omega(\partial\,\mu/\partial\omega) + \mu > 0$. Assuming that ε and μ are simultaneously negative, and multiplying by $-\mu$ and $-\varepsilon$, respectively, we can write

$$\omega\left(\varepsilon\frac{\partial\mu}{\partial\omega} + \mu\frac{\partial\varepsilon}{\partial\omega}\right) + 2\mu\varepsilon < 0,$$

where it is now understood that in this expression both ε and μ are positive quantities. For $n^2 = \mu\varepsilon$, it follows that

$$\omega\frac{\partial n^2}{\partial\omega} + 2n^2 = n\left(\omega\frac{\partial n}{\partial\omega} + n\right) < 0,$$

where we recognize the group index $n_{\rm G} = \omega(\partial n/\partial\omega) + n$. Therefore, the condition that energy should always be positive leads to a condition on the product of phase and group indices, namely $n\,n_{\rm G} < 0$. Since we have assumed conditions consistent with a NIM, where $n < 0$, it must follow that the group index is positive.

3 An example of ordinary refraction

Before we proceed with the study of the interaction of a pulse with a NIM, we set out to establish a standard baseline of what is meant by ordinary refraction using the formalism developed above. In Fig. 3 we illustrate a case where a pulse crosses from vacuum into a *dispersion-less* material such that $\varepsilon = 4\mu = 1$, and so $n = 2$. The pulse diameter (which is specified in space and then advanced in time) when the field amplitude is approximately 1/e of the on-axis value is roughly $30\lambda_{\rm p}$, which translates into a pulse 30 wave cycles ($\lambda_{\rm p}/c$) in duration. Because the pulse width is more than several wavelengths, we avoid the extra complications of diffraction, at least for short propagation distances on the order of just a few pulse widths: the incident wavefront is, and remains, nearly plane.

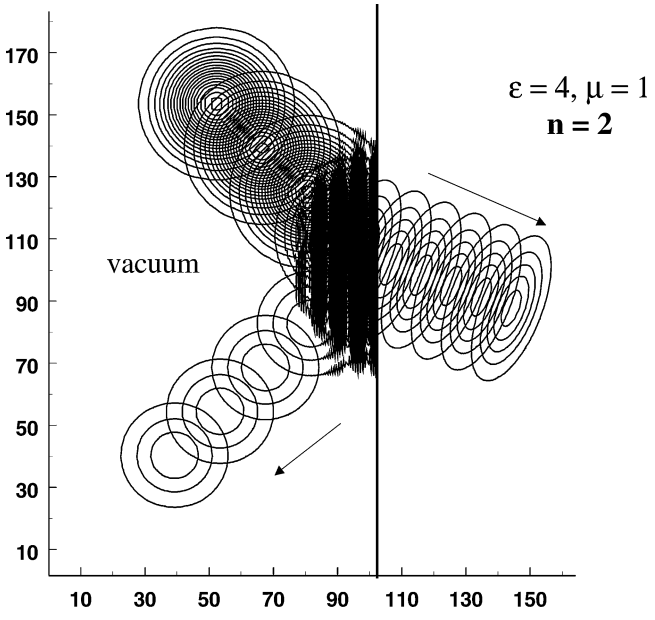

FIGURE 3 Electric field of a pulse approximately 100 fs in duration traversing an interface that separates vacuum from a dispersion-less medium that has $\varepsilon = 4\mu = 1$. This figure represents ordinary refraction between two positive-index materials. The *arrows* indicate the direction of energy flow for both the transmitted and reflected components. The pulse is compressed along the direction of motion as a result of slowing down to a speed of c/n

As expected, the pulse becomes compressed into an ellipse whose major axis is perpendicular to the direction of propagation. Almost immediately the energy velocity acquires a value of $c/2$, as expected. This slow-down reflects largely a loss in forward momentum, although parts of the initial momentum and energy are back-reflected at the interface. Snell's law predicts that a beam incident at 45 degrees will refract into the high-index material at an angle of approximately 20.7 degrees. The refraction angle (i.e. the direction of energy flow) can be easily found by monitoring the two components of electromagnetic momentum that enter the right half space (RHS) as a function of time, namely

$$P_{\tilde\xi}(\tau)_{\rm RHS} = \frac{1}{c^2}\int_{\tilde\xi=0}^{\tilde\xi=\infty}\int_{\tilde y=-\infty}^{\tilde y=\infty} S_{\tilde\xi}(\tilde y,\tilde\xi,\tau)\,{\rm d}\tilde y\,{\rm d}\tilde\xi$$

and

$$P_{\tilde y}(\tau)_{\rm RHS} = \frac{1}{c^2}\int_{\tilde\xi=0}^{\tilde\xi=\infty}\int_{\tilde y=-\infty}^{\tilde y=\infty} S_{\tilde y}(\tilde y,\tilde\xi,\tau)\,{\rm d}\tilde y\,{\rm d}\tilde\xi. \qquad (10)$$

In Fig. 4 we plot typical results for $P_{\tilde\xi}(\tau)_{\rm RHS}$ and $P_{\tilde y}(\tau)_{\rm RHS}$ as functions of time, in units of $1/c^2$. The momenta are seen to build up until the entire pulse has entered the medium. At steady state, the refraction angle can be calculated as $\theta_{\rm r} = \tan^{-1}\left(P_{\rm y}/P_{\rm z}\right)$, which in our example yields the same results predicted by Snell's law to at least two parts in a thousand.

There are some aspects of this dynamics that we would like to present now which we believe will help us to better understand the negative-refraction process. We wish to address the dynamics of the interaction of the pulse as it evolves in

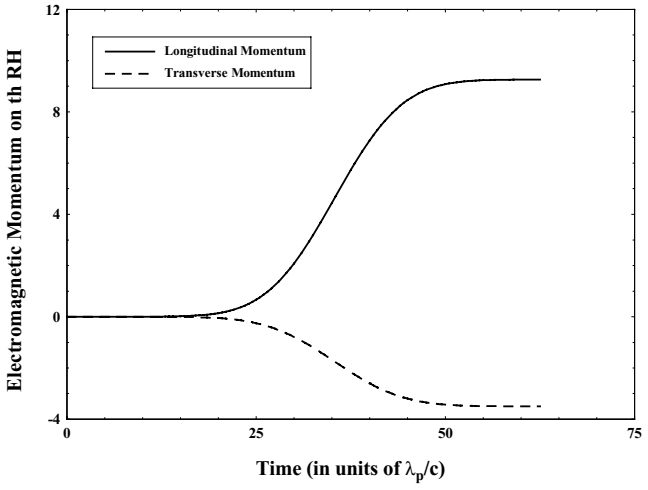

FIGURE 4 Typical total electromagnetic momenta as given by Eq. (11) for the case of Fig. 3, calculated as a function of time as the pulse transits across the interface. The build up is followed by a steady-state condition, which gives the final values of the momenta. Those steady-state values are then used to calculate the refraction angle. In this case the results predicted by Snell's law are reproduced with an accuracy of two parts in a thousand, even for such short pulses

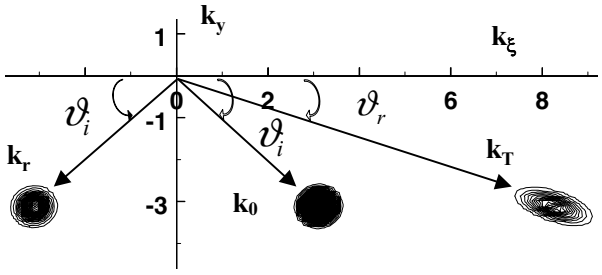

FIGURE 5 The k-space representation of the scattering depicted in Fig. 3. We show the initial and scattered wave packets, which completely identify the wave vectors involved in the interaction. The ellipse on the *right-hand side* takes on such a shape as a consequence of the spatial compression that the field is subjected to, in order to satisfy the Fourier condition that ties real to conjugate space, i.e. $\delta k \delta \xi \sim$ constant

Fourier space, by plotting the power spectrum, which we define as $|E(k_{\tilde{y}}, k_{\tilde{\xi}})|^2$ for the initial and scattered pulses. In general, the input wave packet is centered at $\mathbf{k}_0 = k_0(\cos\vartheta_i\mathbf{k} - \sin\vartheta_i\mathbf{j})$. The scattering produces a reflected wave packet, centered at $\mathbf{k_r} = k_0(-\cos\vartheta_i\mathbf{k} - \sin\vartheta_i\mathbf{j})$, and a transmitted wave packet, centered at $\mathbf{k}_T = k_0 n(\cos\vartheta_r\mathbf{k} - \sin\vartheta_r\mathbf{j})$, where ϑ_r is the angle of refraction. As can be easily verified, this leaves the transverse component of the wave vector unchanged. We depict this situation in Fig. 5. As the pulse of Fig. 3 enters the high-index material, its velocity is reduced, and it forms an ellipse whose major axis is normal to the direction of propagation, as shown. At the same time, the k-space wave packet must also distort accordingly, and it forms an ellipse whose major axis points in the direction of motion: the major axis of the ellipse of the wave packet in k-space is normal to the major axis of the ellipse that the field forms in real space.

In Fig. 6 we show the disposition of the phase fronts within the last snapshot of the field of Fig. 3. The figure suggests that the wavefronts remain plane during the entire interaction, which is what one might expect for a non-diffracting

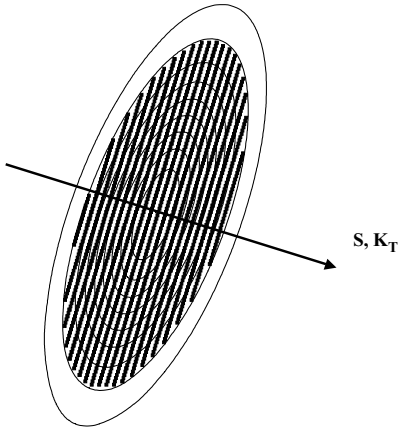

FIGURE 6 Pulse electric field intensity distribution for the final snapshot of Fig. 3. With knowledge of the field amplitude and phase, we show the position of the zero-degree phase planes. We note that the direction of energy (**S**) flow coincides with the direction of the wave vector $\mathbf{K}_T$. In addition, the phase planes are perpendicular to the direction of $\mathbf{K}_T$, a result consistent with the fact that the pulses are not diffracting over the propagation distances we are considering

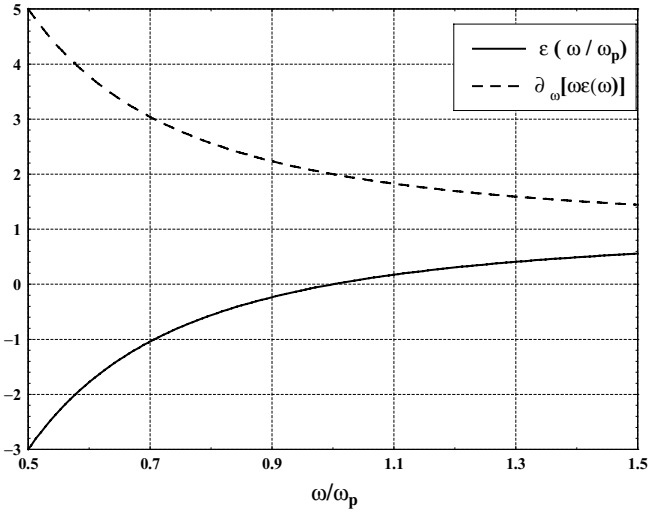

FIGURE 7 Dielectric susceptibility and permeability as given in Eq. (1) (*solid line*). The *dashed curve* represents the derivative $\partial\,[\,\omega\varepsilon(\omega)\,]/\partial\omega$, which we easily identify with the group velocity in the special case of $\varepsilon = \mu$

pulse, as the transmitted wave vector remains normal to those planes. Therefore, Figs. 3–6 provide a complete picture of the scattering process, with a description of the fields in real and conjugate space, as well as a description of the phase fronts, and this is the sort of information one needs in order to build a more complete, self-consistent picture of the dynamics for a pulse that traverses a NIM interface.

4 Propagation into a NIM: normal incidence

The discussion of how a pulse traverses a NIM boundary is perhaps best handled by first studying the case of normal incidence. In Fig. 7 we show the material dispersion curves, along with the behavior of $\partial\,[\,\omega\varepsilon(\omega)\,]/\partial\omega = \partial\,[\,\omega\mu(\omega)\,]/\partial\omega$, which determine the group (or energy) velocity of the pulse once it has transited into the NIM. We tune the carrier frequency to $\tilde{\omega} = 0.7$, where $\varepsilon(\omega) = \mu(\omega) = -1$, and $\partial\,[\,\omega\varepsilon(\omega)\,]/\partial\omega = \partial\,[\,\omega\mu(\omega)\,]/\partial\omega = 3$. The dynamics of the entire pulse is shown in Fig. 8. The pulse slows down to an energy (or group) velocity of $c/3$, and reflections are negligible. Since we have chosen a pulse wide enough so

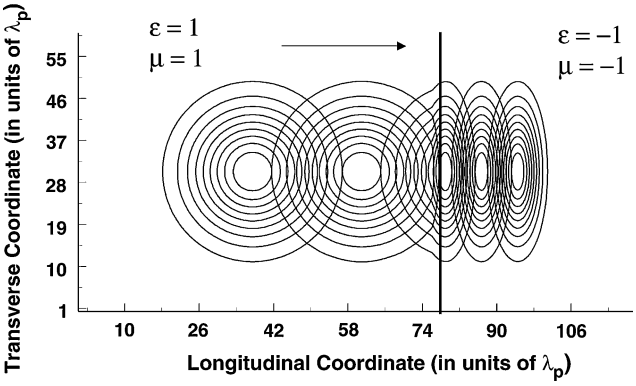

FIGURE 8 A 100-wave-cycle pulse crosses from vacuum into a NIM at normal incidence

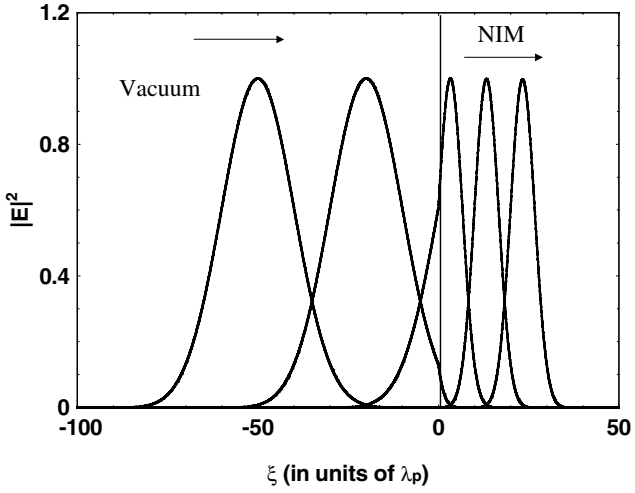

FIGURE 9 Longitudinal cross section of the pulse depicted in Fig. 8. The only significant effect is that the pulse slows down

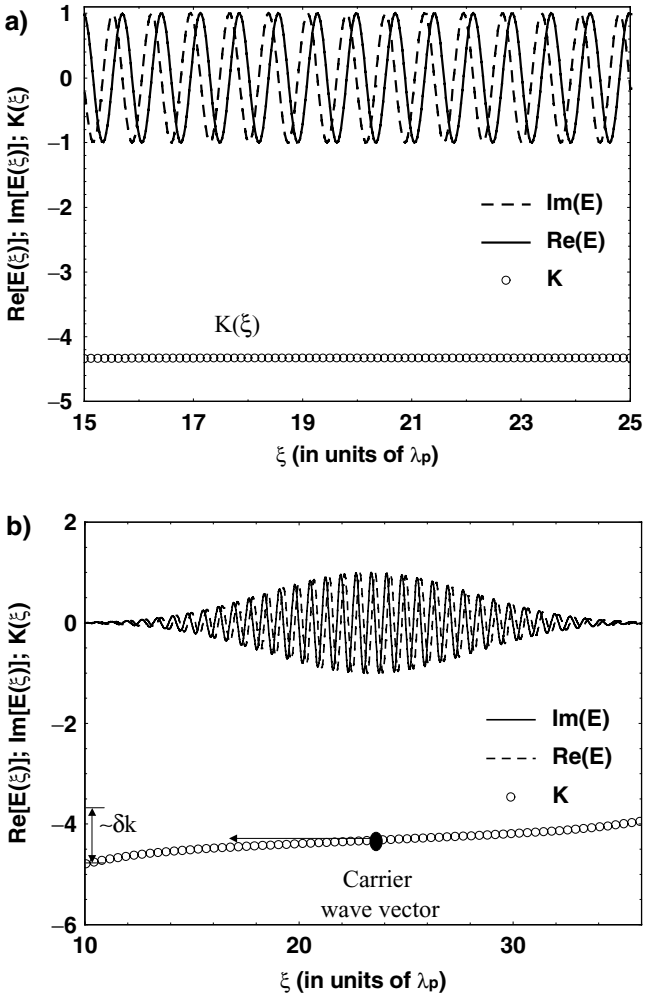

FIGURE 10 **a** Real and imaginary parts of the electric field inside the NIM, as a function of position. Knowledge of the field amplitude and phase as a function of position and time allows us to extract a local, instantaneous wave vector K as a function of position. For a nearly CW pulse there is only the carrier wave vector. Note that it is negative. **b** Same as (**a**), but for an incident pulse approximately 30 wave cycles in duration. It is evident that the carrier wave vector can be associated with a part of the pulse where the field is most intense. The presence of an imparted chirp is also evident. The *amount* of chirp imparted is similar to the amount of chirp imparted to the pulse of Fig. 1, because both pulses propagate with the same speed and undergo similar spatial compression. However, in this case it is opposite in sign (*positive slope*), while for the case of Fig. 1 the carrier wave vector of the transmitted pulse is clearly positive

that diffraction does not occur over the propagation distances of interest, we select the on-axis, longitudinal slice of the pulse, and monitor its propagation. For normal incidence, the longitudinal component of the magnetic field H_z can be neglected, and Eqs. (9) reduce to a set of two coupled equations. In Fig. 9 we plot the on-axis electric field intensity at different times, as the pulse enters and settles into the NIM. The magnetic field undergoes similar development.

We now seek information about the field's phase, and try to correlate it to its power spectrum. The field envelope is a complex function, namely

$$E(\xi,\tau) = |E|e^{i\varphi(\xi,\tau)} = E_r + iE_i. \tag{11}$$

Since reconstruction of the total field requires us to take into account the carrier wave vector of the original expansions Eqs. (5), the total instantaneous, local wave vector can be obtained by calculating the derivative of the phase in Eq. (11) and by adding the initial free-space wave vector $\mathbf{k}_0$: $K(\xi,\tau) = k_0 + \partial\varphi(\xi,\tau)/\partial\xi$. Using Eq. (11) one can easily show that in terms of the field components

$$\frac{\partial\varphi(\xi,\tau)}{\partial\xi} = \frac{E_i\partial_\xi E_r - E_r\partial_\xi E_i}{E_r^2 + E_i^2}, \tag{12}$$

where ∂_ξ indicates differentiation with respect to ξ. In Fig. 10 we show E_r, E_i, and K as functions of position, for the time that corresponds to the last snapshot of propagation inside the NIM for two cases: CW (long super-Gaussian excitation), Fig. 10a, and pulsed dynamics, Fig. 10b, respectively. The figures reveal that K is negative in both instances, but while it is constant for the CW beam, K increases linearly with position inside the pulse. The carrier wave vector is found in the dominant part of the pulse, near its center, and the spatial phase of the pulse picks up a chirp that causes the pulse to significantly broaden in k-space. The amount of broadening, δk, can be estimated by taking the difference in K between the beginning and the end of the pulse, as indicated in the figure. In Fig. 11a we show the power spectrum of input and output pulses for $\varepsilon = 1\mu = 1$. We remark that: (i) the output wave packet is a superposition of purely negative wave vectors, consistent with Fig. 10, and that a simple comparison between the locations of the input and scattered wave packets makes this look like a reflection event. We remind the reader that this wave packet is moving forward, as shown in Fig. 9. (ii) A comparison between the input and output wave packets reveals spectral broadening (spatial frequencies) by nearly a factor of three, consistent with the slow down observed and the consequent spatial compression of the field observed in Fig. 9. (iii) The slope of the chirp is positive. Under ordinary conditions (e.g. Fig. 1), the chirp has a negative slope, and decreases with position. Since propagating further into the material does not change the bandwidth of the transmitted pulse, we conclude that geometrical dispersion at the interface is solely responsible for the dynamics just described.

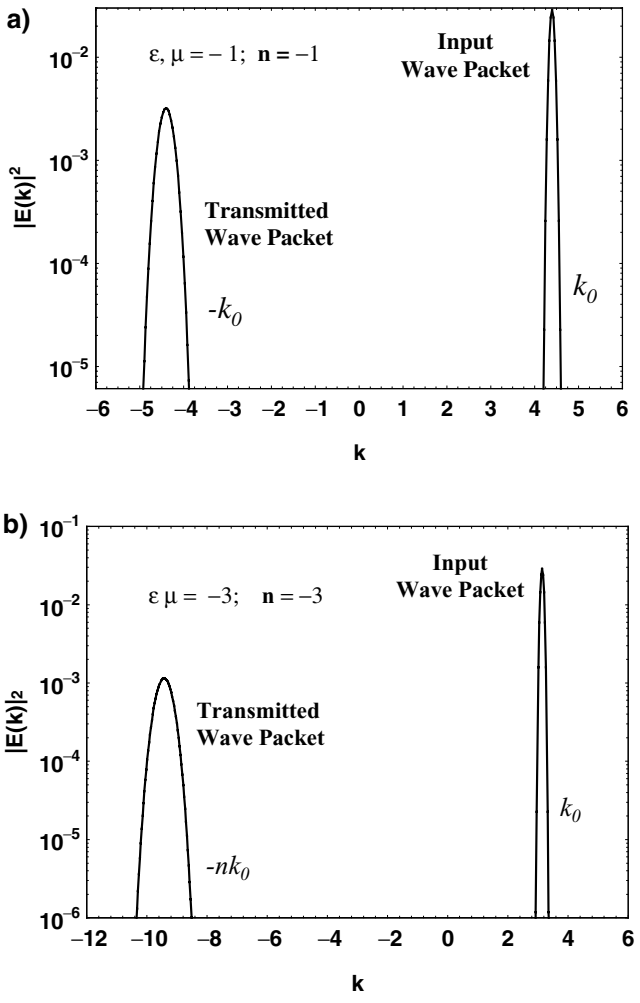

FIGURE 11 **a** Fourier decomposition of the incident and scattered (*electric field*) pulses of Figs. 9 and 10b. This figure is the shorthand version of Fig. 10b, because it immediately gives the component wave vectors and the broadening associated with the geometrical dispersion triggered by the interface crossing. **b** Same as (**a**) but with $\varepsilon = \mu = -3$, and a group velocity of $\partial\,[\,\omega\varepsilon(\omega)\,]/\partial\omega = 5$. The pulse broadens as a result of an increased index discontinuity, and not as a result of material dispersion

In Fig. 11b we show what happens to the input and scattered wave packets when $\tilde{\omega} = 0.5$, for which $\varepsilon(\omega) = \mu(\omega) = -3$ and $\partial\,[\,\omega\varepsilon(\omega)\,]/\partial\omega = \partial\,[\,\omega\mu(\omega)\,]/\partial\omega = 5$. In this case the pulse slows down to $c/5$, reflections are still negligible for normal incidence, and the power spectrum is broadened by approximately a factor of five with respect to the incident wave packet. We also note that once again the carrier wave vector (or peak of the wave packet in the figure) is located at negative frequencies, and it is centered at $-nk_0$, which is the correct magnitude of the wave vector in a material with index $-n$.

As we have seen, the presence of chirp in the transmitted pulse is a clear indication that by crossing a single interface the pulse experiences significant geometrical dispersion. Given the unusual characteristics of the interface, and the unusual connotations of the transmitted pulse, unusual broadening of the wave packet and other more uncommon effects should not be surprising. We point out that under the right conditions the presence of chirp can be turned into an asset, and may help explain a number of anomalous effects, ranging from enhanced group delays to negative tunneling times in stratified structures [28]. Therefore, given the right set of circumstances, NIMs may exhibit anything from superluminal group velocities to negative delays, with twists and turns in ways yet to be unraveled.

5 Oblique incidence

At first glance, the case of oblique incidence is the strangest of all. Yet, it is the most interesting because it challenges everything we are accustomed to. We use the parameters of Fig. 9, with $\tilde{\omega} = 0.7$, $\varepsilon(\omega) = \mu(\omega) = -1$, $\partial\,[\,\omega\varepsilon(\omega)\,]/\partial\omega = \partial\,[\,\omega\mu(\omega)\,]/\partial\omega = 3$, and launch the pulse at an angle of 45 degrees with respect to the normal. The result is depicted in Fig. 12. As the figure shows, the pulse impinges on the surface, and bends upward. The dynamics that ensues causes the longitudinal component of the magnetic field H_z to change sign, thus inverting the direction of the transverse component of the Poynting vector in Eq. (6) and consequently changing the sign of the transverse electromagnetic momentum in Eq. (10).

Calculation of the refraction angle using the electromagnetic momenta of Eq. (10) reveals it to be approximately 45 degrees, as predicted by Snell's law by putting $n = -1$. In fact, we find that Snell's law continues to be a good indicator of the refraction angle even for pulses only a few wave cycles in duration, for all angles investigated. Calculation of the energy velocity then reveals that the pulse settles into the NIM at a speed of $c/3$. Figure 12 also suggests that the pulse becomes distorted while it propagates at speeds well below the speed of light in vacuum. The slight interference pattern near the NIM surface on the vacuum side suggests the existence of back-scattered waves. We note that unlike the case of PBG structures, the transition into the NIM material is quite smooth, as we do not observe the kind of trapping near the

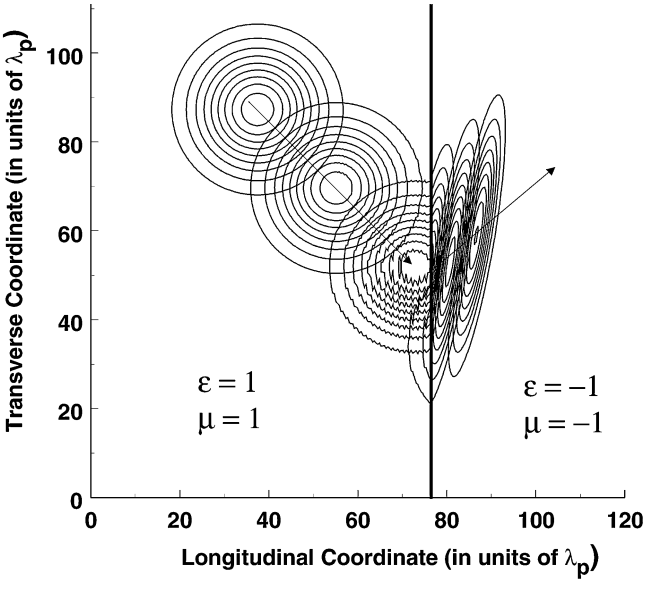

FIGURE 12 Same as Fig. 8, but with an incident angle of 45 degrees. The manifestation of negative refraction is a clear consequence of the integration of Eqs. (9), assuming a Drude-like dispersion model, and no absorption. Using the electromagnetic momentum formalism of Eqs. (10), the refraction angle is calculated to be 45 degrees, as predicted by Snell's law and an index of refraction $n = -1$

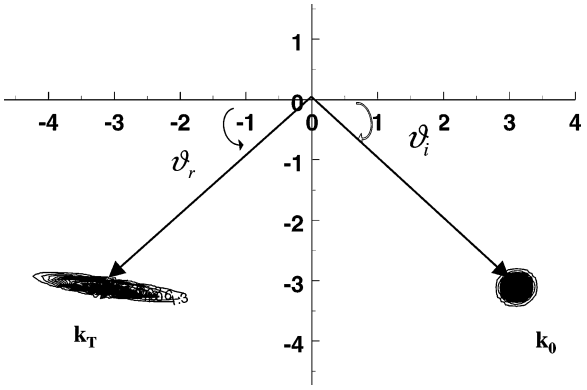

FIGURE 13 The scattering of Fig. 12 is represented in k-space. This figure immediately gives the wave-vector decomposition of the wave packet of Fig. 12: all its components are negative wave vectors, elongated in such a way that its major axis forms a 90 degree angle with the wave packet of physical space. Clearly, this diagram shows that given the degree of available k-vectors, it is possible to mold geometrical dispersion (i.e. arrange a periodic structure of some sort) to affect the outcome of the interaction

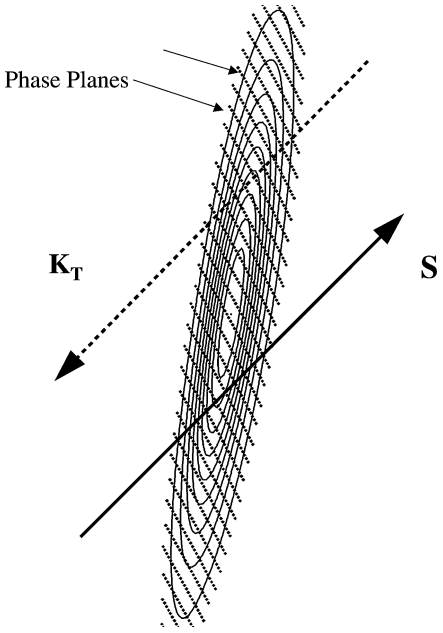

FIGURE 14 Calculated phase fronts for the pulse of Fig. 12 (*dashed, parallel lines that traverse the pulse ellipse*). The planes of constant phase (in this case zero phase) are normal to the carrier wave vector $\mathbf{K}_\mathrm{T}$. The phase fronts re-align themselves in order to maintain their natural tendency to remain orthogonal to the carrier wave vector. The fact that we now have an angular spread of wave vectors implies that there are some slight distortions of the phase fronts, which become less noticeable as pulse duration is increased, but may become important if shorter pulses, higher-order dispersion, or diffraction come into play

surface, inside the structure, as reported for a PBG structure with negative effective index [18], although the end result may be the same.

In Fig. 13 we show the incident and scattered wave packets in Fourier space. The longitudinal component of the wave vector has inverted its sign, thus making the forward-moving packet wave a superposition of purely negative wave vectors. We remark that the transmitted wave packets in Figs. 12 and 13 are rotated in the same direction as for the normal refraction process depicted in Figs. 3–5. The phase planes, which we show in Fig. 14, re-align themselves to safeguard their natural tendency to remain normal to the carrier wave vector, $\mathbf{K}_\mathrm{T}$. We note that they indeed appear to swing around a pivot point as they cross the interface. However, at best this dynamics might suggest superluminal phase velocity, which is meaningless from the standpoint of energy transport.

Given the dynamics depicted in Figs. 12–14, we may draw several conclusions. (i) In terms of pulse shape, the transmitted ellipse of Fig. 12 appears to be oriented in the same way as in the case of normal refraction, Fig. 3. In this sense one may argue that the pulse re-shapes and positions itself as it would under normal conditions. (ii) The phase planes re-orient themselves to maintain their orthogonality with the carrier wave vector, although a range of wave vectors are generated as a result of pulse compression and re-shaping. (iii) The pulse is strongly re-shaped, refracts in the negative direction, but always travels at speeds well below the speed of light in vacuum. It does so in a predictable way, as suggested by Eqs. (9), which also suggest that for propagation in a homogenous medium both group and energy velocities always remain subluminal. This may change in the case of stratified media, where we expect significant departures between the two velocities [25].

6 Concluding remarks

Using newly derived equations of motion, we have shown that, at least in the case of $\varepsilon = \mu$, the group velocity can be obtained from an inspection of the equations of motion, and that it must be positive for any homogenous medium, including NIMs, based on the condition that the electromagnetic energy should always be positive. The transmitted pulse always travels at speeds smaller than the speed of light in vacuum, and undergoes significant re-shaping as its phase fronts are re-aligned to maintain their orthogonality with the carrier wave vector. The pulse becomes compressed, acquires a chirp, and is manifestly a superposition of negative wave vectors even though it propagates in the positive direction. It can also be argued that the study of a single interface crossing reveals dynamical aspects that can be lost if one attempts to study more complicated geometries. Finally, although the similarities with multidimensional, positive-index PBGs are useful and the speculative process constructive, our analysis suggests that analogies should only be carried so far, as generalizations and conclusions for PBGs are of limited validity when applied to materials that have simultaneously negative permittivity and permeability.

REFERENCES

1 V.G. Veselago, Sov. Phys. Usp. **10**, 509 (1968)
2 R.A. Shelby, D.A. Smith, S. Schultz, Science **77**, 292 2001; C.G. Parazzoli et al., Phys. Rev. Lett. **90**, 107 401 (2003)
3 J.B. Pendry, A.J. Holden, D.J. Robbins, W.J. Stewart, IEEE Trans. Microwave Theory Tech. **47**, 2075 (1999)
4 J.B. Pendry, Phys. Rev. Lett. **85**, 3966 (2000)
5 N. Garcia, M. Nieto-Vesperinas, Opt. Lett. **27**, 885 (2002); N. Garcia, M. Nieto-Vesperinas, Phys. Rev. Lett. **88**, 207 403 (2002)
6 P.M. Valanju, R.M. Walser, A.P. Valanju, Phys. Rev. Lett. **88**, 187 401 (2002); P.M. Valanju, R.M. Walser, A.P. Valanju, Comment, Phys. Rev. Lett. **90**, 029704 (2003)

7 J.B. Pendry, D.R. Smith, Comment, Phys. Rev. Lett. **90**, 029703 (2003)
8 (i) D.R. Smith, N. Kroll, Phys. Rev. Lett. **85**, 2933 (2000); (ii) R.W. Ziolkowski, A.D. Kipple, Phys. Rev. E **68**, 026615 (2003); (iii) R.W. Ziolkowski, E. Heyman, Phys. Rev. E **64**, 056625 (2001)
9 R.W. Ziolkowski, Phys. Rev. E **64**, 046604 (2001); S.D. Gupta, R. Arun, G.S. Agarwal, Phys. Rev. B **69**, 113 104 (2004)
10 R.W. Ziolkowski, Opt. Express **11**, 662 (2003)
11 D.R. Smith, D. Schurig, J.B. Pendry, Appl. Phys. Lett. **81**, 2713 (2002); S. Cummer, Appl. Phys. Lett. **82**, 2008 (2003)
12 P.W. Milonni, G.J. Maclay, Opt. Commun. **228**, 161 (2003)
13 D.R. Fredkin, A. Ron, Appl. Phys. Lett. **81**, 1753 (2002)
14 V.M. Agranovich, Y.R. Shen, R.H. Baughman, A.A. Zakhidov, Phys. Rev. B **69**, 165 112 (2004)
15 I.V. Shadrivov, A.A. Sukhorukov, Y.S. Kivshar, Phys. Rev. E **67**, 057602 (2003)
16 Focus issue on negative refraction and metamaterials. Opt. Express **11**, 639 (2003) and references therein
17 C. Luo, S.G. Johnson, J.D. Joannopoulos, J.B. Pendry, Opt. Express, **11**, 746 (2003); C. Luo, S.G. Johnson, J.D. Joannopoulos, Appl. Phys. Lett. **81**, 2352 (2002)
18 S. Foteinopoulou, E.N. Economou, C.M. Soukoulis, Phys. Rev. Lett. **90**, 107 402 (2003)
19 M. Centini, C. Sibilia, M. Scalora, G. D'Aguanno, M. Bertolotti, M.J. Bloemer, C.M. Bowden, I. Nefedov, Phys. Rev. E **60**, 4891 (1999)
20 M. Scalora, M.J. Bloemer, A.S. Manka, S.D. Pethel, J.P. Dowling, C.M. Bowden, J. Appl. Phys. **83**, 2377 (1998); M.J. Bloemer, M. Scalora, Appl. Phys. Lett. **72**, 1676 (1998)
21 http://www.utexas.edu/research/cemd/nim/index.html. Web site maintained by the authors of Ref. [6] above
22 L.D. Landau, E.M. Lifshitz, *Electrodynamics of continuous media*, Pergamon, Press 1960 edition, pp. 253–256
23 J.D. Jackson, *Classical Electrodynamics*, 2nd edn. (Wiley, New York, 1975), Chap. 6
24 A. Yariv, P. Yeh, *Optical Waves in Crystals* (Wiley, New York, 1984), Chap. 6
25 G. D'Aguanno, M. Centini, M. Scalora, C. Sibilia, M.J. Bloemer, C.M. Bowden, J.W. Haus, M. Bertolotti, Phys. Rev. E **63**, 036610 (2001)
26 M. Scalora, M.E. Crenshaw, Opt. Commun. **108**, 191 (1994)
27 W.H. Press, S.A. Teukolsky, W.T. Vetterling, B.P. Flannery, *Numerical Recipes in C: The Art of Scientific Computing*, 2nd edn. (Cambridge University Press, 1997)
28 M. Centini, M.J. Bloemer, K. Myneni, M. Scalora, C. Sibilia, M. Bertolotti, G. D'Aguanno, Phys. Rev. E **68**, 016602 (2003); G. D'Aguanno, M. Centini, M.J. Bloemer, K. Myneni, M. Scalora, C.M. Bowden, C. Sibilia, M. Bertolotti, Opt. Lett. **27**, 176 (2002); M.J. Bloemer, K. Myneni, M. Centini, M. Scalora, G. D'Aguanno, Phys. Rev. E **65**, 051615 (2002)